Organic LETTERS

Letter

pubs.acs.org/OrgLett

Computational Study with DFT and Kinetic Models on the Mechanism of Photoinitiated Aromatic Perfluoroalkylations

Victor M. Fernández-Alvarez,[†] Manuel Nappi,[†] Paolo Melchiorre,*[,†,‡] and Feliu Maseras*[,†,§]

[†]Institute of Chemical Research of Catalonia (ICIQ), Avgda. Països Catalans 16, 43007 Tarragona, Catalonia, Spain

[‡]Institució Catalana de Recerca i Estudis Avançats, Passeig Lluís Companys 23, 08010 Barcelona, Spain

[§]Departament de Química,Universitat Autònoma de Barcelona, 08193 Bellaterra, Catalonia, Spain

Supporting Information

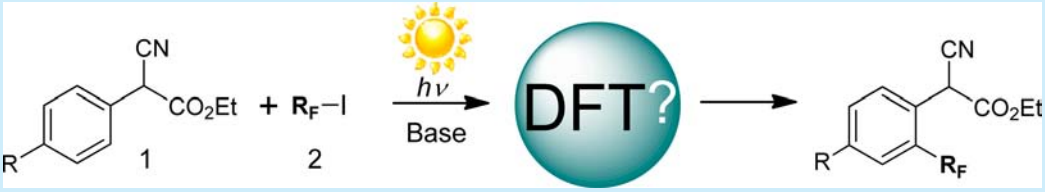

ABSTRACT: A combination of DFT calculations and kinetic models is applied to fully elucidate the seemingly complex reactivity of α-cyano arylacetates toward metal-free photoinitiated aromatic perfluoroalkylation. The resulting mechanistic framework rationalizes the observed quantum yield as well as the differences in reactivity and/or selectivity of seemingly similar substrates. The use of a kinetic model for the chemical interpretation of the DFT-computed reaction constants is shown to be critical.

The past few years have witnessed a resurgence of interest in visible light-driven photoreactions.[1] Synthetic chemists recognize that light excitation can open new dimensions to chemistry, since molecular excited states can react in completely different ways compared with the ground state. In addition, visible light photochemistry holds great potential for the design of more sustainable and environmentally responsible chemical processes.[2] This has resulted in the recent development of a variety of synthetically valuable photochemical reactions, mainly exploiting the ability of photoredox-active transition-metal complexes to excite organic molecules toward the generation of radical intermediates.[3] Recently, it was demonstrated that the photochemical activity of electron donor−acceptor (EDA) complexes,[4] molecular aggregations which occur upon interaction of organic substrates, can also serve to photogenerate open-shell reactive species under mild reaction conditions.[5]

Despite the synthetic potential of these photochemical strategies, the mechanistic determination of a light-driven reaction can be challenging, because of the presence of multistep transformations involving transient intermediates. Computational chemistry is an established and useful complement to experiment in dealing with mechanistic complexity,[6] but its application in photochemical synthetic processes has remained largely underdeveloped so far. The main obstacle to a more widespread application of calculations to photochemical reaction mechanisms concerns the intrinsic complexity of the electronic excited states involved. The appropriate tools for the quantum-mechanical description of processes in the excited states are ab initio multiconfigurational methods,[7] which however become too computationally demanding for most of the systems of practical use. Density functional theory (DFT), in particular time-dependent DFT (TD-DFT), is a useful technique in the characterization of the excitation process, and it has been applied with success to the description of charge-transfer (CT) states,[8] free radical systems, and redox electron transfer.[9] However, the evolution of the excited state after the excitation remains a challenge for DFT. We notice, however, that the electronically complex part of a photochemical process is often limited to a few steps after the excitation. Usually, the evolution of the system rapidly leads to a new ground-state intermediate, which undergoes a specific reactivity amenable to exploration by conventional DFT approaches.

In this work, we successfully applied DFT methods to elucidate the mechanism and understand the origin of the regioselectivity of the photochemical aromatic perfluoroalkylation of ethyl α-cyano phenylacetate **1** (Scheme 1). This metal-free, light-driven process, recently reported by some of us,[10] has two appealing features that make it suitable as test system for the

Scheme 1. Model Reaction for the Visible-Light-Mediated Aromatic Perfluoroalkylation of α-Cyano Arylacetates[a]

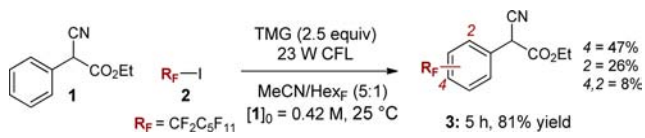

[a]CFL: compact fluorescent light; TMG: 1,1,3,3-tetramethyl guanidine; Hex_F: tetradecafluorohexane.

Received: April 13, 2015
Published: May 14, 2015

DOI: 10.1021/acs.orglett.5b01069
Org. Lett. 2015, 17, 2676−2679

efficiency of DFT modeling: (i) the availability of a variety of experimental mechanistic data, and (ii) the existence of some experimental observations that remain unexplained. We realize that this particular system may be amenable to a more sophisticated multiconfigurational method, but the calculation would be much more expensive, and one of our goals is to prove that this more elaborate description is not necessary for this particular case.

The perfluoroalkylation proceeds regioselectively at the aromatic ring of **1** to give the *para* and *ortho* functionalized products **3** in a 2:1 ratio, with a minor amount of the *ortho*−*para* bifunctionalized adduct. A quantum yield (Φ) of 3.8 was determined (λ = 400 nm), suggesting a radical chain mechanism as the main reaction pathway. The proposed mechanism (Scheme 2), distilled out from experimental observations, was

Scheme 2. Preliminary Radical Chain Mechanistic Proposal[10]

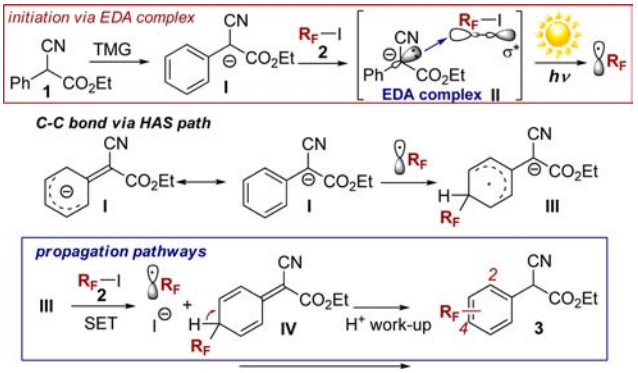

based on a homolytic aromatic substitution (HAS)[11] pathway initiated by the photochemical activity of the EDA complex of type **II**, formed by the aggregation of the enolate-type compound **I** (generated upon deprotanation of **1** from 1,1,3,3-tetramethyl guanidine, TMG) with the perfluorohexyl iodide **2**. A visible-light-driven single electron transfer (SET) led to the formation of radical species R_F•, which then reacted with the arene within the enolate **I** to form the new C−C bond. The mesomeric effect of the anionic substituent in **I** facilitated the C−C bond formation leading to the cyclohexadienyl radical anion **III**. A SET to **2** was proposed as the propagation step of the radical chain, with the intermediate **IV** which was eventually deprotonated to form the final arene product **3**.

There are, however, some mechanistic aspects that remain obscure and difficult to ascertain by purely experimental approaches. In particular: (i) why the reaction takes place with perfect regioselectivity for the aromatic ring of **1**, while the plausible formation of the α-carbonyl perfluoroalkylated adduct **4** was not observed (Figure 1a); (ii) why is the process completely inhibited by small changes in the reactant **1**, i.e., replacement of the cyano group by NO_2, CO_2Et or a keto moiety (Figure 1b); in addition, α-*para*-nitrophenylacetate **5** behaves in a completely different manner under the same reaction conditions, the perfluoroalkylation taking place exclusively at the sp^3 carbon leading to product **6** (Figure 1c); the origin of this divergence in regioselectivity remains unclear; and (iii) Finally, what are the factors inducing a quantum yield of about 4, a relatively small value for an HAS-type transformation.[12] In order to answer these questions, we carried out a thorough DFT investigation of the system with calculations in solvent using the

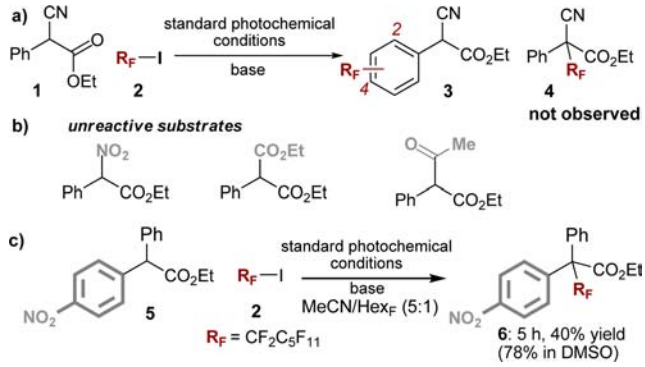

Figure 1. Additional experimental evidence. Standard photochemical conditions refer to those explicitly mentioned in Scheme 1, including the presence of a TMG base to deprotonate the substrate.

ωB97X-D functional. Full computational details are provided in the Supporting Information.

We chose a model system where perfluoropropyl iodide (C_3F_7I, **2a**) was used as the alkylating agent. The computed mechanism is summarized in Scheme 3. The first step is the

Scheme 3. DFT Computation of the Mechanism[a]

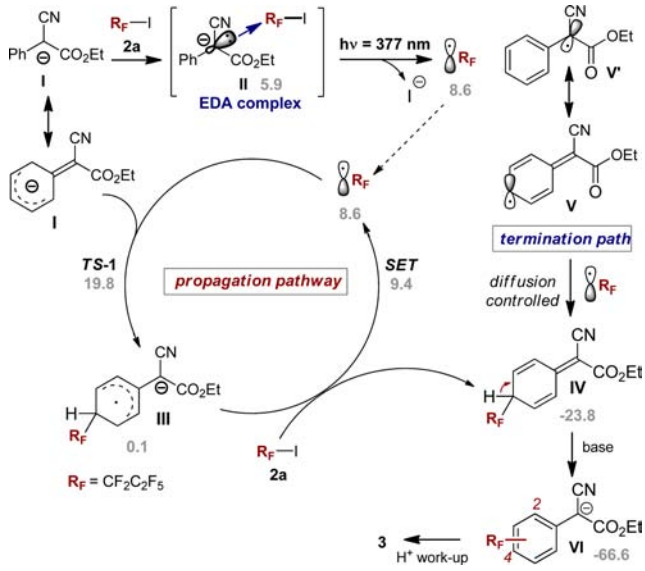

[a]Free energies (gray color) in kcal·mol^{-1}.

formation of the EDA complex **II**, generated upon aggregation of the enolate **I** and **2a**, which then undergoes a photoinduced ET. The existence of the EDA complex was confirmed by calculation. A minimum was found where the shorter distances between fragments, around 3.8 Å are between the carbon attached to iodine and the phenyl ring. Through a TD-DFT calculation, we found a HOMO−LUMO CT transition with a maximum absorption at λ = 377 nm. Although not necessarily very accurate because of the lack of vibronic corrections, it must be mentioned that this vertical excitation energy is not in disagreement with the experimental UV−vis spectrum. The excited EDA has an initial energy 75.8 kcal·mol^{-1} above the reactants (5.9 kcal·mol^{-1} for the EDA complex **II** in the ground state). The excited state resulting from the vertical excitation can be clearly characterized as an open-shell singlet. Our attempts to optimize its geometry as an open-shell singlet state within the TD-DFT framework failed, because of the difficulty to retain the same excited state from one

DOI: 10.1021/acs.orglett.5b01069
Org. Lett. 2015, 17, 2676−2679

optimization step to the next. These other excited states are however not relevant to the excitation process because they have oscillator strength of zero. This technical problem prompted us to estimate the behavior of the electronic state resulting from the vertical excitation by studying the triplet state. The triplet state geometry optimization leads to the barrierless breakdown of the excited EDA adduct into three fragments: the radical intermediate **V**, the radical perfluoropropyl R_F•, and the iodide anion. Two mechanistically relevant bifurcations take place at this point, and we will analyze them separately. First, we will discuss the propagation/termination dichotomy, while the regioselectivity issue, associated with which of the possible resonance forms of the substrate (**I** vs **I′** or **V** vs **V′**) better describes the reaction, will be considered later.

Concerning the propagation/termination dichotomy, R_F• can combine with **V** to form the intermediate **IV** (termination path), which can easily lose a proton to restore aromaticity and form the HAS product **3** (upon protonation of the intermediate **VI**). This termination step has no significant barrier and is expected to be diffusion controlled. Alternatively, the enolate **I** can trap R_F• to form the anionic intermediate **III** through the transition state **TS-1** (structure shown in Figure S6 in the Supporting Information). The intermediate **III** can transfer an electron via SET to **2a** to form a new R_F• (propagation path) and the intermediate **IV**. The barrier for the SET step was computed applying the Marcus theory in the form detailed in the Supporting Information. This SET step will not be further discussed because the barrier is too low to affect the reaction outcome. It must be mentioned that the computed barrier for the SET was introduced in the kinetic model and confirmed to be not critical.

The highest energy point in the propagation cycle is in the transition state **TS-1** leading to **III**, 19.8 kcal.mol^{-1} above the reactants, thus 9.2 kcal·mol^{-1} above the intermediate R_F•. The competition between the chain propagation manifold (9.2 kcal·mol^{-1} barrier) and the termination pathway (barrierless, diffusion-controlled) directly influences the quantum yield of the overall process. If we were to evaluate this competition from a pure comparison of the highest free energy points, as it is often the case for competing processes in homogeneous catalysis,[13] the conclusion would be that the radical coupling dominates, with no chain propagation taking place. This scenario would call upon a quantum yield $\leq$1, which is in sharp disagreement with the experimentally determined quantum yield of $\approx$4. This treatment is however plagued by the large difference in the concentration of the species involved. The enolate **I**, the key intermediate involved in the chain propagation path, arises from an almost quantitative deprotonation of the substrate **1** from TMG, while the radical intermediate **V** (involved in the termination) is a transient species.[14] In order to take concentration differences into account, we carried out a kinetic simulation.[15] Details on the simulation and the estimation of the quantum yield are described in the Supporting Information. We would like to remark that this problem could not be solved by changing the standard state to a different concentration because the real concentration of the intermediates involved in the reaction is not known beforehand. The kinetic simulation requires a rate constant for the combination of R_F• and **V** to form **IV**, which is barrierless in the potential energy surface.[16] We used an experimental estimation of the rate constant for diffusion-controlled radical reactions in a polar solvent, which has been reported to oscillate between 2×10^9 to 1×10^{10} M^{-1} s^{-1}.[17] The estimated quantum yield, which strongly depends on such rate constant, ranges from 3 to 71. This value is in reasonable agreement with the experimental quantum yield, considering the approximations made in the simulation and that this parameter is very sensitive to small changes in energy barriers.

Regarding the selectivity issue, experimentally we observed that the HAS product **3** was exclusively formed with a *para*/*ortho* ratio of 2:1, and no α-carbonyl perfluoroalkylated product **4** was observed (Figure 1a). The regioselectivity-determining step is the trap of the perfluoroalkyl radical by the intermediates **I** and **V**. The barriers for the radical trapping step from **I**, determined for all possible products, are $\Delta G^{\ddagger}$ = 11.2, 11.7, and 20.8 kcal·mol^{-1} for *para*-**3**, *ortho*-**3** (the HAS products), and **4** (the α-carbonyl-functionalized product), respectively. The calculated free energy barriers are in very good agreement with the experimentally observed regioselectivity. The origin of this selectivity was investigated by carrying out a distortion/interaction analysis[18] on the corresponding transition states. This analysis, fully outlined in the Supporting Information, indicates that key factor precluding the attack to the α-carbonyl position (to give **4**) is the large cost for the distortion of the anionic fragment **I** associated with this pathway.

We next tested the ability of our computational approach to reproduce the reactivity of other enolates bearing similar electron-withdrawing groups than **I**, which have however afforded different experimental results (Figure 1b,c). The nitro-substituted enolate **Ia**, where the cyano moiety has been replaced with a nitro group, remained completely unreacted under the standard reaction conditions. We found two conformations for the enolate **Ia** having comparable energies (Figure 2).

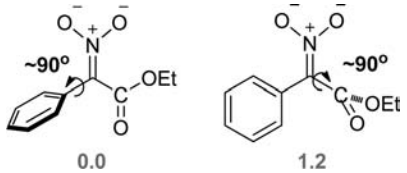

Figure 2. Conformations of **Ia**. Free energies in kcal·mol^{-1}.

These conformations are true minima and differ by 1.2 kcal·mol^{-1} in energy. The TD-DFT calculation indicates that the maximum wavelengths of absorption for the EDA complexes, arising from aggregation of these two conformations with R_F-**I**, are 266 and 299 nm, respectively. As a result, the system no longer absorbs visible light. The initial electron transfer between the reactants does not take place, and the whole process is aborted. Responsible of the hypsochromic shift is the reduced conjugation within **Ia**, since the steric hindrance of the nitro group breaks the planar π system and reduces the delocalization.

The last test for our computational treatment comes from the experiments presented above for α-paranitrophenylacetate **5** (Figure 1c). The challenge here is to reproduce the different regioselectivity of the process. The TD-DFT calculation indicates that the EDA complex between the enolate of **5** and **2** absorbs at λ = 388 nm, thus in the UV−vis region. The transition states leading to the HAS adduct (not observed experimentally) and product **6** have relative energies of 13.8 and 7.1 kcal·mol^{-1}, respectively, thus reproducing the experimentally observed product distribution. The inversion in regioselectivity with respect to α-cyano phenylacetate **1** can be explained by comparing the HOMO of the enolates **I** and **Ib**, derived from **1** and **5**, respectively (Figure 3). The HOMO for **I** has a significant component in the phenyl ring, which is substantially reduced in

DOI: 10.1021/acs.orglett.5b01069
Org. Lett. 2015, 17, 2676−2679

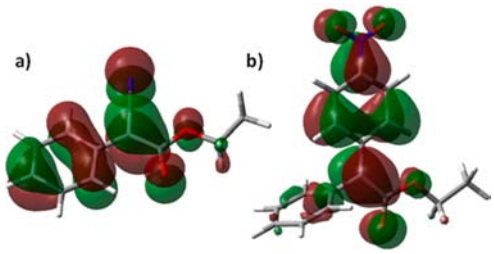

Figure 3. HOMO of the enolates **I** (a) and **Ib** (b).

Ib. As a result, **Ib** has to pay an electronic reorganization penalty to reach the transition state for the HAS process. It is worth mentioning that the small participation of the phenyl ring in the HOMO of **Ib** finds its origin in the same 90° dihedral rotation of the arene reported above for the nitro-substituted enolate **Ia**. In the case of **1a**, steric hindrance from the nitro group distorts the π system and breaks the delocalization, shifting the CT transition of the EDA to the ultraviolet. The same distortion occurs for **Ib**, although, in this case, the nitrophenyl ring allows for a greater delocalization so that the excitation by visible light is still possible.

In summary, we have demonstrated that mostly ground-state DFT calculations can successfully complement experiments in the mechanistic elucidation of a photochemical synthetic process. The quantum yield above 1 was properly rationalized after treating the rate constants emerging from the DFT results with a kinetic model, which was critical to address this problem. The potential of the computational approach was further confirmed by explaining the nontrivial outcomes of enolates bearing different electron-withdrawing groups. Specifically, the discordant regioselectivity of **Ib** with respect to **I** was explained on the basis of the shape of the HOMO orbital of the species reacting with R_F•. Our results show that DFT calculations can be a useful tool in the study of photochemical processes, even with their limitations in the treatment of the evolution of excited states. The main practical problems are in fact not related to the DFT calculation itself, but to its connection with experimental results, which in this case required the use of a kinetic model in order to reproduce the quantum yield. The mechanistic clarification of this process can open the way for future improvements in related processes and expands the scope of computational chemistry for treating photochemical processes. It is true that light is only used to generate the initial radicals in this system, but the reported mechanism is likely to share features with other photoinitiated processes that suggest a prominent role for kinetic models in their computational description.

■ ASSOCIATED CONTENT

Supporting Information

Experimental procedures, computational details, full computed free energy profiles, other computational data, and Cartesian coordinates for all optimized structures. The Supporting Information is available free of charge on the ACS Publications website at DOI: 10.1021/acs.orglett.5b01069.

■ AUTHOR INFORMATION

Corresponding Authors

*E-mail: pmelchiorre@iciq.es
*E-mail: fmaseras@iciq.es

Notes

The authors declare no competing financial interest.

■ ACKNOWLEDGMENTS

Financial support from the ICIQ Foundation, MINECO (project CTQ2014-57661-R and Severo Ochoa Excellence Accreditation 2014-2018 SEV-2013-0319) and the European Research Council (ERC Starting Grant no. 278541-ORGA-NAUT to P.M.) is gratefully acknowledged. V.F. is grateful to MINECO for a FPI fellowship (ref BES-2012-057655). M.N. is grateful to MINECO for a FPU fellowship (ref AP2010-1963).

■ REFERENCES

(1) (a) Schultz, D. M.; Yoon, T. P. *Science* **2014**, *343*, 1239176. (b) *Handbook of Synthetic Photochemistry*; Albini, A., Fagnoni, M. eds.; Wiley-VCH: Weinheim, 2010.
(2) (a) Balzani, V.; Credi, A.; Venturi, M. *ChemSusChem* **2008**, *1*, 26−58. (b) Yoon, T. P.; Ischay, M. A.; Du, J. *Nat. Chem.* **2010**, *2*, 527−532.
(3) (a) Prier, C. K.; Rankic, D. A.; MacMillan, D. W. C. *Chem. Rev.* **2013**, *113*, 5322−5363. (b) Narayanam, J. M. R.; Stephenson, C. R. J. *Chem. Soc. Rev.* **2011**, *40*, 102−113.
(4) (a) Mulliken, R. S. *J. Am. Chem. Soc.* **1952**, *74*, 811−824. (b) Foster, R. *J. Phys. Chem.* **1980**, *84*, 2135−2141. (c) Rosokha, S. V.; Kochi, J. K. *Acc. Chem. Res.* **2008**, *41*, 641−653.
(5) (a) Arceo, E. I.; Jurberg, D.; Álvarez-Fernández, A.; Melchiorre, P. *Nat. Chem.* **2013**, *5*, 750−756. (b) Arceo, E.; Bahamonde, A.; Bergonzini, G.; Melchiorre, P. *Chem. Sci.* **2014**, *5*, 2438−2442.
(6) Sameera, W. M. C.; Maseras, F. *WIREs Comput. Mol. Sci.* **2012**, *2*, 375−385.
(7) (a) Domcke, W.; Sobolewski, A. L. *Nat. Chem.* **2013**, *5*, 257−258. (b) Vela, S.; Mota, F.; Deumal, M.; Suizu, R.; Shuku, Y.; Mizuno, A.; Awaga, K.; Shiga, M.; Novoa, J. J.; Ribas-Arino, J. *Nat. Commun.* **2014**, *5*, 4411. (c) Cox, N.; Retegan, M.; Neese, F.; Pantazis, D. A.; Boussac, A.; Lubitz, W. *Science* **2014**, *345*, 804−808.
(8) (a) Laurent, A. D.; Adamo, C.; Jacquemin, D. *Phys. Chem. Chem. Phys.* **2014**, *16*, 14334−14356. (b) Daniel, C. *Coord. Chem. Rev.* **2015**, *282*−*283*, 19−32.
(9) (a) Fantacci, S.; De Angelis, F. *Coord. Chem. Rev.* **2011**, *255*, 2704−2726. (b) Ma, J.; Su, T.; Li, M.-D.; Du, W.; Huang, J.; Guan, X.; Phillips, D. L. *J. Am. Chem. Soc.* **2012**, *134*, 14858−14868. (c) Matt, B.; Xiang, X.; Kaledin, A. L.; Han, N.; Moussa, J.; Amouri, H.; Alves, S.; Hill, C. L.; Lian, T.; Musaev, D. G.; Izzet, G.; Proust, A. *Chem. Sci.* **2013**, *4*, 1737−1745.
(10) Nappi, M.; Bergonzini, G.; Melchiorre, P. *Angew. Chem., Int. Ed.* **2014**, *53*, 4921−4925.
(11) The HAS pathway capitalizes upon the electrophilic nature of perfluoroalkyl radicals, which are eager to react with arenes, see: Studer, A. *Angew. Chem., Int. Ed.* **2012**, *51*, 8950−8958.
(12) For an example of a photo-induced HAS of electron-rich arenes with perfluoroalkyl radicals showing a quantum yield >200, see: Barata-Vallejo, S.; Martín Flesia, M.; Lantaño, B.; Argüello, J. E.; Peñéñory, A. B.; Postigo, A. *Eur. J. Org. Chem.* **2013**, 998−1008.
(13) Balcells, D.; Maseras, F. *New J. Chem.* **2007**, *31*, 333−343.
(14) Fischer, H. *Chem. Rev.* **2001**, *101*, 3581−3610.
(15) (a) Rush, L. E.; Pringle, P. G.; Harvey, J. N. *Angew. Chem., Int. Ed.* **2014**, *53*, 8672−8676. (b) Goehry, C.; Besora, M.; Maseras, F. *ACS Catal.* **2015**, *5*, 2445−2451.
(16) Yang, T.; Parker, D. S. N.; Dangi, B. B.; Kaiser, R. I.; Stranges, D.; Su, Y.-H.; Chen, S.-Y.; Chang, A. H. H.; Mebel, A. M. *J. Am. Chem. Soc.* **2014**, *136*, 8387−8392.
(17) (a) Wojnárovits, L.; Takács, E. *Radiat. Phys. Chem.* **2013**, *87*, 82−87. (b) Elliot, A. J.; McCracken, D. R.; Buxton, G. V.; Wood, N. D. *J. Chem. Soc. Faraday Trans.* **1990**, *86*, 1539−1547.
(18) (a) Morokuma, K. *J. Chem. Phys.* **1971**, *55*, 1236−1237. (b) Bickelhaupt, F. M. *J. Comput. Chem.* **1999**, *20*, 114−128. (c) Schoenebeck, F.; Houk, K. N. *J. Am. Chem. Soc.* **2010**, *132*, 2496−2497.

DOI: 10.1021/acs.orglett.5b01069
Org. Lett. 2015, 17, 2676−2679